In-vivo optical imaging of hsp70 expression to assess collateral tissue damage associated with infrared laser ablation of skin

Gerald J. Wilmink
Vanderbilt University
Department of Biomedical Engineering
Nashville, Tennessee 37235

Susan R. Opalenik
Vanderbilt University
Department of Pathology
Nashville, Tennessee 37235

Joshua T. Beckham
Vanderbilt University
Department of Biomedical Engineering
Nashville, Tennessee 37235

Mark A. Mackanos
Stanford School of Medicine
Stanford, California 94305-5119

Lillian B. Nanney
Vanderbilt School of Medicine
Department of Plastic Surgery
Cell and Developmental Biology
Nashville, Tennessee 37212

Christopher H. Contag
Stanford School of Medicine
Department of Pediatrics, Microbiology and Immunology
Department of Radiology
Stanford, California 94305-5119

Jeffrey M. Davidson
Vanderbilt University
Department of Pathology
Nashville, Tennessee 37235
and
VA Tennessee Valley Healthcare System
Research Service
Nashville, Tennessee 37212

E. Duco Jansen
Vanderbilt University
Department of Biomedical Engineering
Nashville, Tennessee 37235

Abstract. Laser surgical ablation is achieved by selecting laser parameters that remove confined volumes of target tissue and cause minimal collateral damage. Previous studies have measured the effects of wavelength on ablation, but neglected to measure the cellular impact of ablation on cells outside the lethal zone. In this study, we use optical imaging in addition to conventional assessment techniques to evaluate lethal and sublethal collateral damage after ablative surgery with a free-electron laser (FEL). Heat shock protein (HSP) expression is used as a sensitive quantitative marker of sublethal damage in a transgenic mouse strain, with the *hsp70* promoter driving luciferase and green fluorescent protein (GFP) expression (*hsp70A1*-L2G). To examine the wavelength dependence in the mid-IR, laser surgery is conducted on the *hsp70A1*-L2G mouse using wavelengths targeting water (OH stretch mode, 2.94 μm), protein (amide-II band, 6.45 μm), and both water and protein (amide-I band, 6.10 μm). For all wavelengths tested, the magnitude of *hsp70* expression is dose-dependent and maximal 5 to 12 h after surgery. Tissues treated at 6.45 μm have approximately 4× higher *hsp70* expression than 6.10 μm. Histology shows that under comparable fluences, tissue injury at the 2.94-μm wavelength was 2× and 3× deeper than 6.45 and 6.10 μm, respectively. The 6.10-μm wavelength generates the least amount of epidermal hyperplasia. Taken together, this data suggests that the 6.10-μm wavelength is a superior wavelength for laser ablation of skin. [DOI: 10.1117/1.2992594]

Keywords: ablation; free-electron laser; heat shock protein expression; skin; wound healing; bioluminescence; optical imaging.

Paper 07455RR received Nov. 8, 2007; revised manuscript received Aug. 5, 2008; accepted for publication Aug. 15, 2008; published online Oct. 6, 2008.

1 Introduction

The goal of surgical ablation is to remove unwanted 'target' tissue and cause minimal damage to adjacent and underlying biological structures. Lasers are well suited for this task, because their operating parameters can be selected to deliver short, high energy pulses within a focused beam. Such focusing allows for tightly controlled and precise tissue etching.[1–7] The principal parameters that govern laser surgical performance are pulse structure, radiant exposure, and wavelength.[8–10] It has been shown that tissue damage can be minimized by selecting laser pulse durations that are shorter than the thermal relaxation time of tissue.[5] The spread of energy can also be further reduced by tuning the laser wavelength to match regions of strong tissue absorption. Infrared (IR) wavelengths are known to be strongly absorbed by tis-

Address all correspondence to: E. Duco Jansen, Ph.D., Department of Biomedical Engineering, VU Station B #351631, Vanderbilt University, Nashville, TN 37232. Tel 615-343-1911; Fax 615-343-7919; Email: duco.jansen@vanderbilt.edu

1083-3668/2008/13(5)/054066/12/$25.00

Table 1 Infrared wavelengths and corresponding molecular absorption bands. The absorption coefficients given are those for water. For skin, where the water content will be ~75 % the absorption owing to the water content will be proportionally reduced. (*) 6.45 μm, while not directly on a water absorption peak is still strongly absorbed by the symmetric bending mode that peaks at 6.10 μm.

	Infrared wavelength (μm)		
	2.94 μm	6.10 μm	6.45 μm
Primary dermal chromophores			
1. Water (~75 volume)			
Vibrational mode	Symmetric and asymmetric OH stretch	Symmetric bending (v2)	Symmetric bending (v2)
Absorption coefficient (μ_A) ⟨cm^{-1}⟩	12202[48]	2691[48]	825[48]
Optical penetration depth (δ) ⟨μm⟩	1	3.7	12
2. Protein (~25% volume)			
Vibrational mode	NA	Amide-I band, C═O stretch	Amide-II band, N-H plane

sues due to their high water content, and therefore IR laser sources are well suited for medical ablation.[11]

The earliest ablation investigations primarily used laser sources tuned to wavelengths targeting water, the chief tissue chromophore and most efficient absorber of IR radiation.[5,12–20] For instance, the erbium:YAG laser (λ =2.94 μm), which targets the OH-stretch mode of water, has long been used for ablation procedures.[17,18,20] However, despite having high ablation rates and exceedingly small optical penetration depths, many reports indicate that such sources generate large zones of collateral tissue damage.[11,17,18,20] Edwards et al. used the Vanderbilt Mark-III free-electron laser (FEL), an IR laser tunable between 2 and 10 μm, to demonstrate that wavelengths that targeted protein bands (~6 μm) generated less collateral damage than those that targeted water (2.94 μm).[21] This seminal finding was the basis for numerous studies aimed at developing mid-IR lasers as precise surgical tools.[8,9,22–25]

More recent mid-IR ablation investigations have focused on comparing 6.10 and 6.45 μm, wavelengths corresponding to amide-I and amide-II absorption bands of protein, respectively.[8,9,26] Compared to 6.45 μm, a wavelength of 6.10 μm has greater overlap with the bending mode of water and therefore has higher tissue absorption (see Table 1).[27] Due to this fundamental difference, it was initially hypothesized that 6.45 μm may target protein bands more effectively than 6.10 μm, and this superior targeting may lead to greater disruption of the tissue matrix, less violent tissue removal, and less collateral damage.[14] With this in mind, the structural failure of proteins was investigated by analyzing ablation plumes and ejected tissue fragments.[8,27] In contrast, more recent evidence suggests that 6.1 μm is superior, because it gives lower ablation thresholds, higher ablation yields, and less collateral tissue damage in biological tissues.[8,9,26] Despite more than a decade of research, it is still unclear which IR wavelength is truly superior for ablation.

The main goal of this study is to determine the superior IR wavelength for the ablation of skin: 2.94, 6.10, or 6.45 μm. In contrast to previous studies, which solely depended on histological tools to assess damage on excised tissues, we use *in-vivo* optical imaging techniques to quantify damage on living subjects.[8,21] Excised tissue is a suitable model for exploring the biophysical mechanisms of ablation; however, it cannot be used to capture the dynamics of the tissue's repair response. Our optical imaging approach provides a noninvasive way to monitor this acute repair response. This response is important to identify and monitor, as it gives preliminary indication of the ultimate fate of the remaining tissue (e.g., necrosis, apoptosis, etc.). Moreover, considering that the underlying goal of ablation research is to improve the efficiency of clinical procedures, our approach is more akin to a clinical scenario because we evaluate ablation *in vivo*.

To understand how our new approach can be used to evaluate tissue damage, the mechanisms of laser ablation must be introduced. In brief, pulsed laser ablation removes tissue by causing a quick temperature rise within the target tissue, leading to thermal elastic expansion. Heat that remains in the tissue then diffuses beyond the target into adjacent tissues, resulting in temperature gradients extending beyond the exposure point. If cellular temperature gradients exceed 5 to 6 °C, then intracellular proteins begin to partially denature.[28–30] In an effort to counteract this stress, cells elicit a response mechanism that activates the transcription and synthesis of various molecular chaperones, including heat shock proteins (HSPs). The most widely studied and most thermoresponsive HSP family member is *hsp70*.[30] In a previous study, we used a reporter gene system using the *hsp70A1* promoter to drive the expression of firefly luciferase (*luc*) to examine laser effects on cell cultures and engineered skin equivalents. We demonstrated that *luc* can be used as a surrogate marker for *hsp70* activation and as a measure of sublethal cellular damage.[29–31]

In this study, we use an *hsp70A1-luc green fluorescent protein (hsp70A1-L2G)* mouse model and *in vivo* optical imaging techniques to quantitatively and sequentially evaluate thermal damage associated with FEL ablation procedures. Using the FEL at various radiant exposures, the following three wavelengths were studied: 2.94, 6.10, and 6.45 μm. Both *in vivo* bioluminescence imaging (BLI) and confocal fluorescence microscopy were used to visualize and quantify *hsp70* promoter activity in laser-treated dorsum. This approach provided a sensitive, real-time readout of the magnitude of cellular damage *in vivo*. Conventional histological methods were also used to measure the actual depth of tissue injury and to examine the early repair response of the laser-treated tissues. In summary, this study aimed to: 1. examine the spatiotemporal validity of the *hsp70A1-L2G* model using optical imaging methods, 2. investigate the effects that wavelength and radiant exposure have on *hsp70* expression, and 3. determine which mid-IR wavelength is superior for laser ablation of skin.

2 Materials and Methods

2.1 *Animal Model*

All experiments were conducted in accordance with guidelines specified by the Institutional Animal Care and Use Committee (IACUC) at Vanderbilt University. A transgenic mouse strain, in which the *hsp70* promoter drives the expression of luciferase and GFP reporter genes was provided by the Contag Laboratory (Stanford University). A detailed description of this mouse strain can be found in Ref. 32. In brief, these mice have an FVB background and contain an *hsp70* cassette that is located upstream from GFP and luciferase (*luc*) vectors. In this system, whenever *hsp70* mRNA transcription occurs, these bicistronic reporters are also transcribed and translated. As a result, the GFP and luciferase gene products emit light that can be used as a surrogate marker for *hsp70* gene activity levels.[31]

Real-time polymerase chain reaction and bioluminescent imaging (BLI) were used to select an optimum breeding pair from an original cohort of eight *hsp70A1-L2G* founder mice. Male and female founders were paired and their offspring were screened using bioluminescent imaging and genotyping methods. Only female mice between 8 and 10 weeks old were used to minimize age and gender variability. 48 h prior to laser experiments, mice were anesthetized with isoflurane in a vaporizer (Ohmeda, BOC Health Care, United Kingdom). After the mice were sedated, a rectangular area of the dorsal fur was removed using clippers, and remaining hair was removed using depilatory cream. After thoroughly cleaning off any remaining cream using saline moistened gauze, the mice were then returned to animal care for 2 days.

2.2 *Free Electron Laser Operating Parameters*

The FEL was used to make four 6.5×6.5-mm square lesions on the dorsum of each mouse. Wounds were separated by at least 4 mm. The laser was operated at 30 Hz at wavelengths of 2.94, 6.1, or 6.45 μm. Energy was delivered in 5-μs macropulses with pulse energies of 2, 4, 6, 8, 10, 12.5, 15, 20, 22.5, and 25 ± 0.5 mJ. At each wavelength, the collimated beam was focused to a 200-μm Gaussian beam radius using a 50-cm focal length CaF_2 lens, resulting in radiant exposures of 1.59, 3.17, 4.76, 6.35, 7.96, 9.95, 11.94, 15.91, 17.91, and 19.89 J/cm^2. In a previous study, the ablation threshold on mouse skin was found to be 2.5 J/cm^2 at 6.45 μm, 1.0 J/cm^2 at 6.10 μm, and 0.2 J/cm^2 at 2.94 μm.[26] In terms of threshold multiples, 19.89 J/cm^2 equates to roughly 100 times threshold at 2.94 μm, 20 times threshold at 6.10 μm, and 8 times threshold at 6.45 μm.

A standard knife-edge method was conducted to measure the spot size of the Gaussian (TEM_{00}) laser beam at the surface of the mouse dorsum. This method was necessary to correct for spot size variations due to chromatic aberrations by ensuring that a consistent beam radius of $200\ \mu m \pm 10\ \mu m$ was achieved for each experiment. For each wavelength tested, ablation was performed at or immediately past the beam waist (i.e., using a constant spot size with the beam "diverging" inside the tissue).

Mice were positioned on a three-axis translation stage equipped with a black circular mouse holding plate [Fig. 1(a)]. Pulse energies were measured using an EnergyMax 400A energy meter with an LP-50 detector head (Coherent/Molectron, Portland, Oregon). At least four lesions were made ($n \geqslant 4$) for each radiant exposure at each wavelength.

2.2.1 *Computer-guided laser delivery*

The laser beam was delivered with a computer assisted surgical technique (CAST) system.[33] In brief, the CAST system consists of a set of two orthogonal computer-controlled (Labview, National Instruments, Austin, Texas) galvanometer-driven mirrors built into the FEL beam line that allows a user to scan the focused laser beam over the target tissue with a predetermined pattern. The pattern for the lesions in this study was 6.5×6.5 mm. Skin lesions were generated by making a single pass consisting of 15 sweeps. Each sweep was separated by 460 μm and took 1.33 s with a total exposure time of 20 s [Fig. 1(b)]. Pilot studies indicated slight variations in *hsp70* promoter activity between the cephalic and caudal areas on the dorsum; therefore, the anatomical location for each laser treatment was randomized.

To ensure that each transgenic mouse exhibited comparable sensitivity to heat exposure, a positive control was used on each mouse. A set of custom-designed brass rods with a length of 24 cm, surface area of 19.625 mm^2, c =0.377 kJ/kg K, and mass of 37.4 g, was heated to 70 °C in a water bath. 24 h prior to each FEL experiment, a heated rod was applied for 15 s on the posterior dorsum of each mouse [Fig. 1(b)]. Mice exhibiting bioluminescent intensities ranging from 3 to 6×10^7 photons per second (p/s) were considered suitable for experimentation (data not shown).

2.3 *Bioluminescent Imaging*

After the FEL lesions were made, the mice were imaged using a Xenogen IVIS 200 imaging system (Caliper/Xenogen, Alameda, California). 15 min before each imaging session, the mice were injected i.p. with a 15-mg/ml solution of luciferin substrate to yield a dose of 150 mg/kg. Mice were imaged at 0, 2, 5, 7, 9, 12, 15, 17, 21, 24, 36, and 48 h after the start of the FEL procedure. During each imaging session, mice were placed in the imaging chamber on a heated 37 °C stage. Both photographic and bioluminescent images were ac-

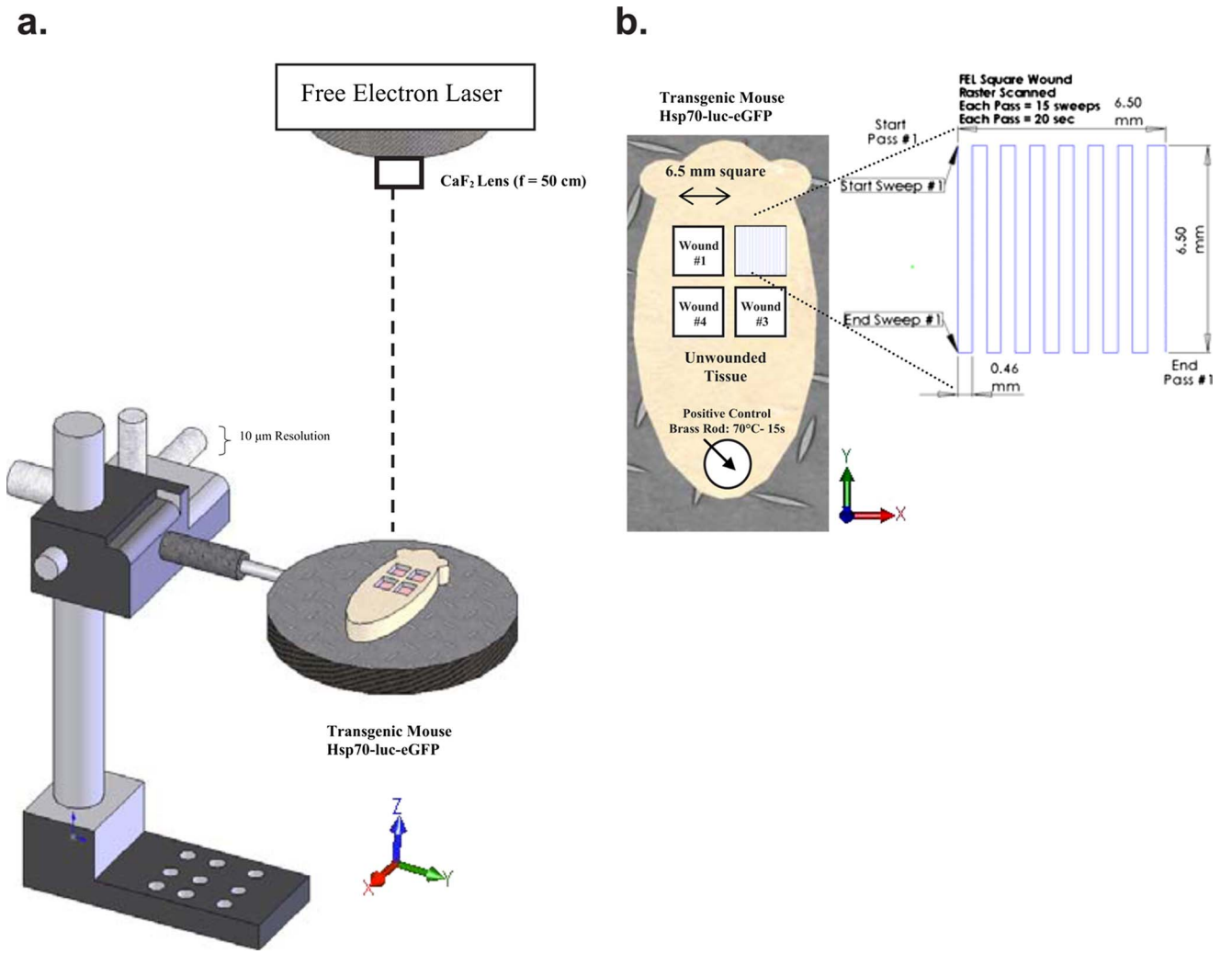

Fig. 1 Schematic representation of experimental methodology. (a) Free electron laser (FEL) optical positioning setup and parameters (λ: 2.94, 6.10, 6.45 μm; H: 1.59, 3.17, 4.76, 6.35, 7.96, 9.95, 11.94, 15.92, 17.91, 19.89 J/cm^2; ω_r: 200 μm±10 μm; τ_p: 5 μs, repetition rate 30 Hz. A 10 week old *hsp70A1*-L2G transgenic mouse was placed and treated on a 20 cm diameter holding plate. (b) Computer-assisted-surgical-technique (CAST) guided FEL wounding.

quired, and each bioluminescent image was superimposed over its corresponding photographic image. Bioluminescent images were integrated over 30 s and the data were represented with a false color scheme representing the regions of varying light emission. Regions of interest (ROIs) encompassed each 6.5×6.5-mm square laser lesion [Fig. 1(b)]. Light emissions from the specified ROIs were then quantified in units of total number of p/s using LivingImage analysis software (v2.12, Xenogen). The light emission from each ROI was then normalized to the light emission recorded from an unwounded section of tissue. This fold-induction value indicated the magnitude of *hsp70* expression generated by the laser treatment.

2.4 *Histology*

A subset of mouse skin samples was harvested for histological analysis. Tissues were examined for cell morphology, degree of damage, and early wound repair response at 12, 48, and 120-h postsurgery. An Olympus Vanox-T AHZ microscope equipped with a Pixera Pro 600 ES camera was used to capture the images. For standard histology, a section of the laser-treated tissue was fixed in formalin, embedded in paraffin, sectioned and stained using hemotoxylin and eosin (HE) and Gomori's trichrome (green) stains.[31] The depth of damage was evaluated using a change in tincture in the Gomori's trichrome stains and was measured using Image-Pro Plus software at a standardized magnification. The magnitude of epidermal hyperplasia was also measured from tissues evaluated at 120-h postsurgery. A portion of each wound was prepared for frozen sectioning in Tissue-Tek® O.C.T.™ compound (Sakura Finetek, Torrance, California), flash frozen in liquid nitrogen, and stored at −70 °C. These sections were used for fluorescence imaging of GFP.

2.5 *Confocal Fluorescence Imaging of hsp70 Green Fluorescent Protein*

Fluorescence imaging of the second bicistronic reporter gene, GFP, was conducted to obtain depth resolved *hsp70* expression. Frozen tissue samples were sectioned with a microtome (10 μm thickness) and imaged using the 5×, 0.15-NA Plan-

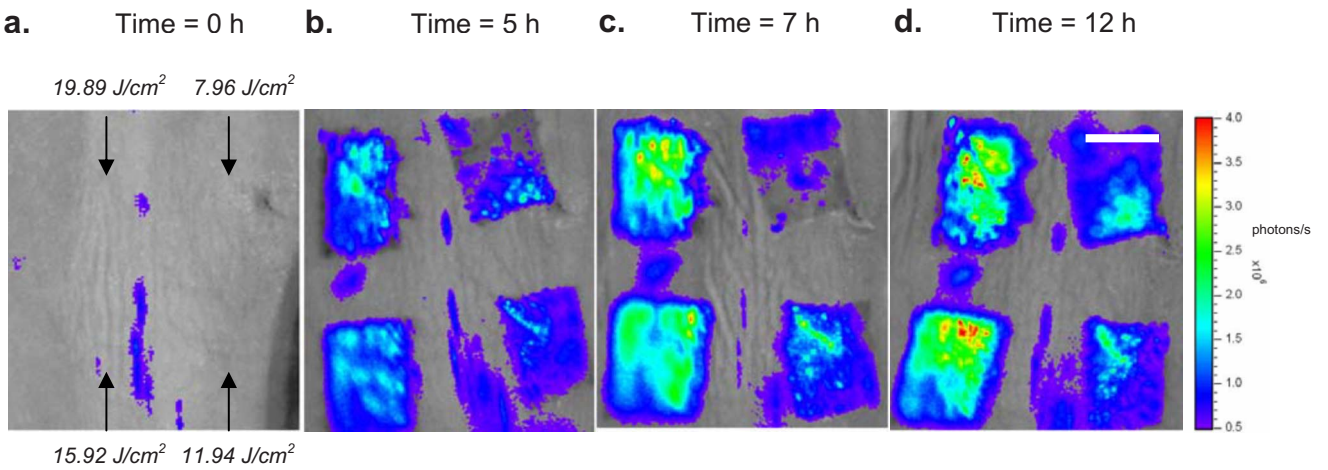

Fig. 2 Visualization of *hsp70* promoter activity on laser-treated mouse skin. Bioluminescent imaging time course of a FEL wounded *hsp70*-luc mouse dermis. (a) Time=0 h. (b) Time=5-h postsurgery. (c) Time=7-h postsurgery. (d) Time=12-h postsurgery. The FEL parameters used to make the wounds were the following: $\lambda = 6.10\ \mu$m, $\omega_t = 200\ \mu$m, $\tau_p = 5\ \mu$s, 30 Hz; H: 7.96, 11.94, 15.92, and 19.89 J/cm^2. Laser-treated tissue has ~18× higher bioluminescence intensities (scale bar=6 mm).

Neofluar objective lens of a Zeiss LSM510 inverted confocal microscope. Samples were excited using a 488-nm argon laser, and the *hsp70*-associated GFP fluorescence was detected using a 505- to 550-nm bandpass filter. Metamorph (Molecular Devices, Sunnyvale, California) was used to quantify signals from the skin's surface to 250 μm below the surface. The GFP signal was measured using rectangular regions of interest ($13 \times 100\ \mu$m). Values represent the mean fluorescence intensity values at three locations for ten different samples. On serial sections of tissue (HE stained), cell counts were measured using Image-Pro Plus (MediaCybernetics, Bethesda, Massachusetts). Cell density was determined using regions of interest with an area 600 μm^2. The fluorescent integrated intensity was then normalized by dividing by the cell density.

3 Results

3.1 *Visualization and Quantification of hsp70 Promoter Activity in Laser-Treated Mouse Dorsum*

A sample of the BLI time-course study of skin treated with the FEL using a wavelength of 6.10 μm and radiant exposures of 7.96, 11.94, 15.92, and 19.89 J/cm^2 is shown in Fig. 2. Prior to surgery, the untreated dorsal skin showed relatively low background bioluminescent intensities, with only minor traces of signal on the skin over the spine [Fig. 2(a)]. Five hours after surgery, significant increases in BL intensities were observed for all laser treatments [Fig. 2(b)]. The 15.92- and 19.89-J/cm^2 exposure sites showed significantly higher expression than sites exposed to 7.96 and 11.94 J/cm^2. For all lesions, the bioluminescent intensities progressively increased after surgery to a maximum intensity at ~12-h postsurgery [Figs. 2(c) and 2(d)].

Figures 3(a)–3(c) show quantitative BLI plotted versus time for each wavelength and radiant exposure tested. hsp70 expression exhibited dose dependency and generally increased with increasing laser radiant exposure, as long as damage was not excessive. For all samples, an initial peak of

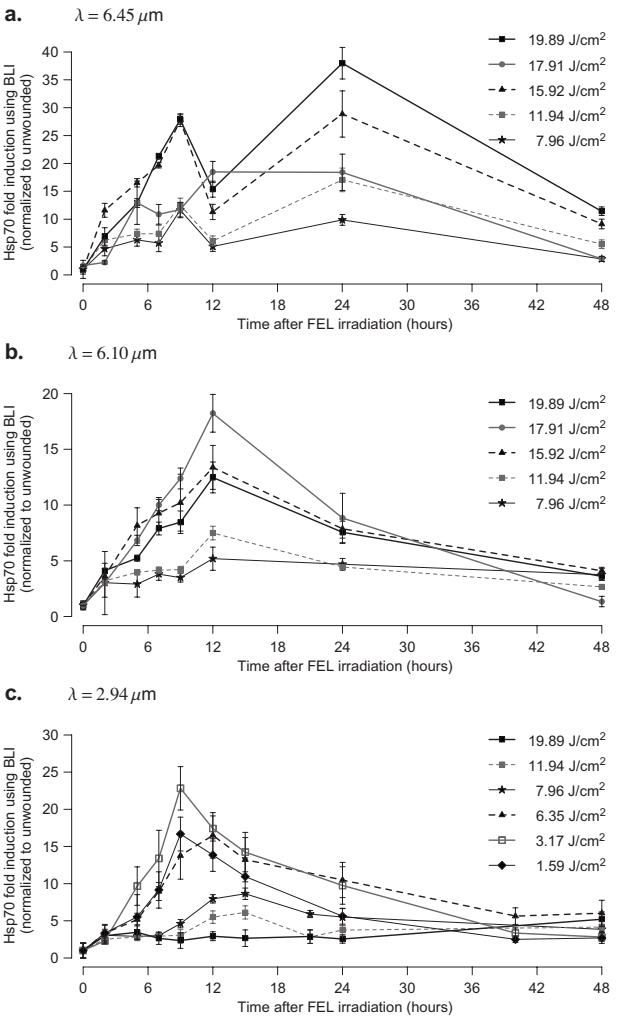

Fig. 3 Quantification of *hsp70* expression using bioluminescent imaging (BLI). *Hsp70* fold-induction (BLI relative to control) plotted versus time. Bioluminescent images were integrated over 30 s. Values are reported as mean±SEM. FEL at (a) $\lambda = 6.45\ \mu$m, (b) $\lambda = 6.10\ \mu$m, and (c) $\lambda = 2.94\ \mu$m.

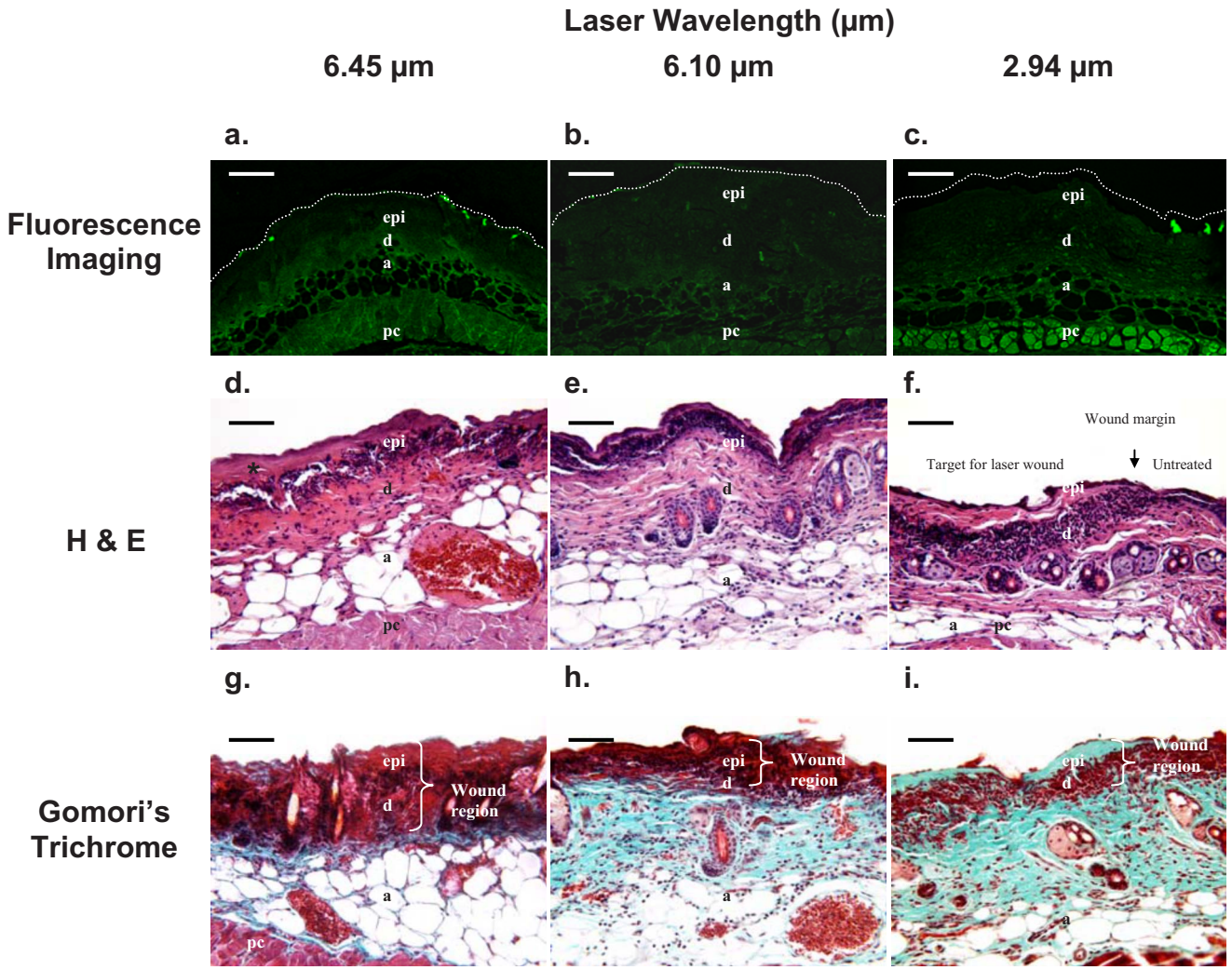

Fig. 4 Morphological methods to measure depth of damage and fluorescent imaging to measure *hsp70* expression. Histology and confocal fluorescence imaging of sections of laser-irradiated dermal tissue. For a consistent comparison, exposures that induced comparable (12-fold) increases in *hsp70* expression are shown. Radiant exposures of 11.94, 15.92, and 1.59 J/cm^2 were used for the wavelengths of 6.45, 6.10, and 2.94 μm, respectively. Tissue was harvested 12-h postinjury. (a), (b), and (c) Fluorescence imaging of *hsp70* induced GFP expression (scale bar =100 μm, epidermis=epi, dermis=d, a=adipose tissue, and pc=panniculus carnosus). (d), (e), and (f) HE stained sections (scale bar=75 μm). (g), (h), and (i) Gomori's (green) trichrome stain is used to visualize the depth of damage of laser-treated tissue (scale bar=75 μm).

hsp70 expression was seen 9- to 12-h postsurgery. At 6.45 μm, a biphasic peak of *hsp70* expression was observed with maxima occurring both 9 and 24 h after laser treatment [Fig. 3(a)]. Increases in radiant exposures from 7.96 to 19.89 J/cm^2 showed 12 to 28 fold-increases in initial *hsp70* expression. At 6.10 μm, a maximum of an 18-fold increase in *hsp70* was obtained with a radiant exposure of 17.91 J/cm^2 [Fig. 3(b)]. Compared to the other wavelengths, the 2.94-μm treatment induced markedly more macroscopic damage to the tissue that manifested itself predominantly as bleeding (data not shown). Therefore, treatments using radiant exposures less than 7.96 J/cm^2 were also tested [Fig. 3(c)]. The magnitude of *hsp70* expression increased as the radiant exposure was increased from 1.59 to 3.17 J/cm^2; however, higher radiant exposures resulted in a decrease in *hsp70* expression.

3.2 *Depth-Resolved hsp70 Expression in Laser-Treated Tissues*

To examine the spatial distribution of *hsp70* expression, GFP signal was evaluated using fluorescence microscopy. Such analyses allowed us to develop a 3-D representation of *hsp70* expression after FEL ablation. Sample confocal fluorescence images (cross sections) of each laser-treated tissue are shown in Figs. 4(a)–4(c). The tissue treated with 6.45 μm had modest signal throughout, and the highest signals appeared in the reticular dermis and cutaneous muscle (panniculus carnosus). The epidermis and papillary dermis were lethally damaged to a depth of approximately 100 μm, as evidenced by the absence of GFP expression. This dark area where GFP expression is minimal correlates to the region of observed tissue damage. Compared to the 6.45-μm treated samples, significantly lower GFP expression was observed in the tissues

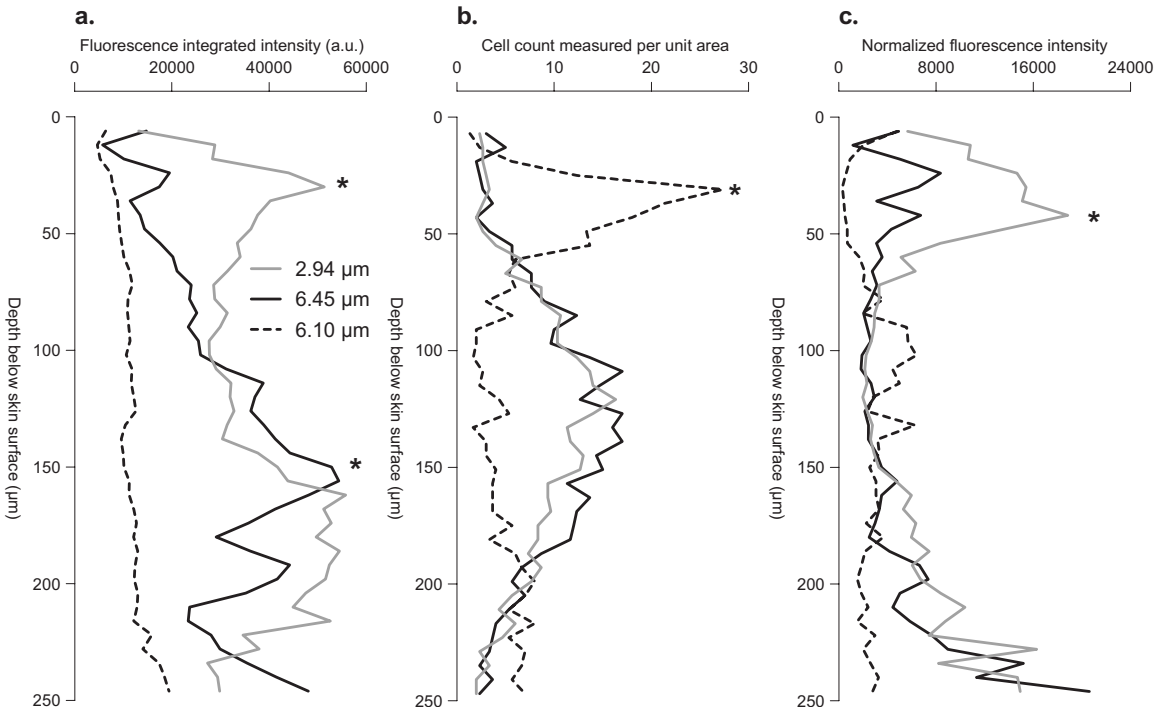

Fig. 5 Quantification of fluorescence signal. (a) Fluorescent integrated intensity versus depth of tissue (μm). Fluorescent intensity was integrated within rectangular regions of interest (13×100 μm) going from the skin surface ($z=0$ μm) to the muscle ($z=250$ μm). Mean fluorescence intensity is plotted and the SD $<5\%$ (SD not plotted for clarity). (b) Average cell number per area versus depth of tissue. (c) The fluorescent intensity values plotted in (a) were normalized to the cell numbers in (b) and plotted as function of tissue depth.

treated with 6.10 μm [Fig. 4(b)]. In the 2.94-μm irradiated samples, considerable expression was observed in the epidermis, superficial dermis, and subdermal muscle [Fig. 4(c)].

To compare the laser treatments, the magnitude of GFP reporter expression was quantified with respect to depth [Fig. 5]. In Fig. 5(a), the integrated fluorescent intensities are plotted versus tissue depth. At 2.94 μm, peak GFP emission was biphasic, with maxima at 40 and 150 μm below the skin surface (marked with an *). In contrast, at 6.45-μm, GFP expression was lowest closest to the skin surface and increased with depth to a maximum at 150 μm. Compared to the other wavelengths, the 6.10-μm wavelength had significantly less signal at all depths. In Fig. 5(b), the cell density is plotted versus depth. At 6.10 μm, the highest density of cells appeared approximately 40 μm below the surface. In contrast, the 2.94- and 6.45-μm treatments showed the highest cell densities approximately 100 to 150 μm below the surface. The data suggest that 6.10 μm promoted less cell death or more cellular migration to the skin surface than the other two wavelengths. Quantitative fluorescence intensities were then normalized to cell density, and these normalized fluorescence values are plotted versus depth in Fig. 5(c). The wavelengths of 2.94 and 6.45 μm showed biphasic peaks occurring at 50 and 250 μm below the surface, while the 6.10-μm treatment had peak expression from 100 to 150 μm below the skin surface.

3.3 *Histological Analysis of Laser-Induced Damage*

Tissues were compared histologically at laser conditions that showed a 12-fold induction of *hsp70* expression 9 to 12 h after laser surgery, based on the results from [Figs. 3(a)–3(c)]. Radiant exposures of 11.94, 15.92, and 1.59 J/cm^2 were compared for wavelengths of 6.45, 6.10, and 2.94 μm, respectively. Cellularity and damage (mechanical and thermal) were visualized using an HE stain [Figs. 4(d)–4(f)] and a Gomori's trichrome stain [Figs. 4(g)–4(i)]. Figures 4(d)–4(f) indicate marked differences between the histological characteristics of samples exposed to the three wavelengths. The 6.45-μm treatment showed the thickest superficial layer of coagulation (see asterisk) [Fig. 4(d)]. Figures 4(g)–4(i) reveal marked differences in tissue damage patterns. The intense green staining of collagen with trichrome is indicative of normal nondisrupted collagen, and the transition to red is indicative of collagen denaturation. The tissues exposed to 6.45 μm showed the deepest zones of collagen denaturation, and the 6.10-μm wavelength showed the shallowest depth of collagen damage.

For all of the wavelengths tested, the depth of damage was dose-dependent, with higher radiant exposures showing deeper damage. The measured depth of damage was plotted versus FEL radiant exposure (J/cm^2) [Fig. 6(a)]. Interestingly, at a given radiant exposure, the depth of damage with 2.94 μm was $\sim 3\times$ that at 6.10 μm, and $\sim 2\times$ that at 6.45 μm.

3.4 *Effects of Laser Wavelength and Radiant Exposure on the Magnitude of hsp70 Expression*

The peak magnitudes of *hsp70* expression were measured and plotted versus laser radiant exposure (J/cm^2) [Fig. 6(b)]. For

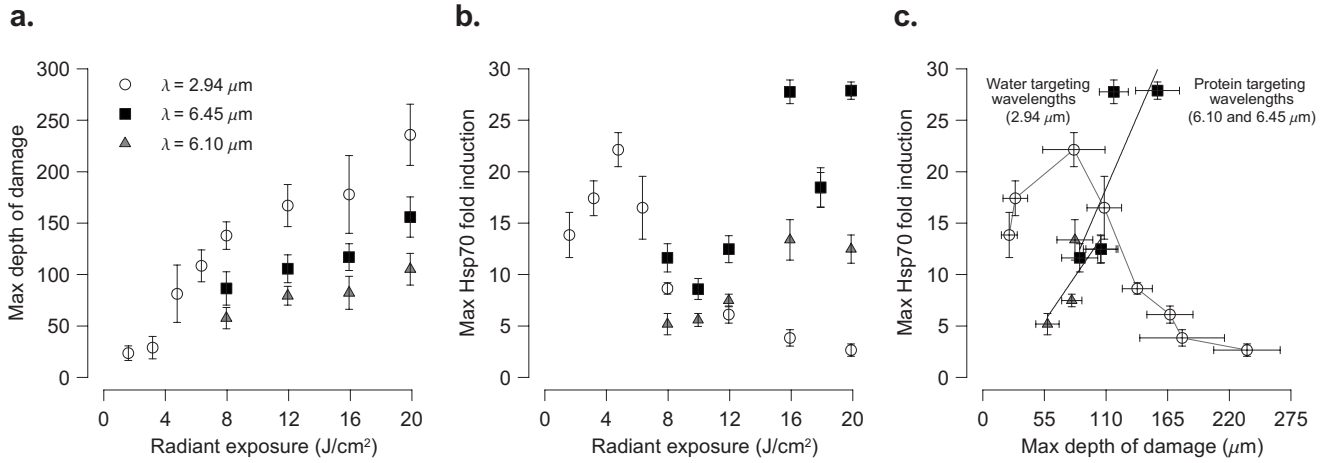

Fig. 6 Collateral thermal damage. (a) The max depth of damage at 12 h plotted versus radiant exposure (J/cm^2). Higher FEL radiant exposures cause deeper tissue damage. At a given radiant exposure the 2.94-μm treatment damages ~2× deeper than 6.45 μm and ~3× deeper than 6.10 μm. Depth of damage was measured from tissue sections using histological stains (Gomori's trichrome). The max depth of damage is expressed as mean±SD, n=90. (b) Peak *hsp70* fold-induction is plotted versus radiant exposure (J/cm^2) for 2.94, 6.10, and 6.45 μm. (c) Peak *hsp70* fold-induction plotted versus depth of tissue damage (μm). The data for 6.45 and 6.10 μm lie on the same line (black dotted line). The 2.94-μm data are shifted (i.e., more hsp70 expression for a given depth of damage) for radiant exposures up to 4.76 J/cm^2 (gray dotted line), and then shows a decrease in hsp70 expression for higher radiant exposures (and deeper depths) that is not seen in either 6.10- or 6.45-μm irradiated tissues.

all wavelengths tested, increased radiant exposures led to increased *hsp70* expression. However, at 2.94 μm, a maximum *hsp70* expression of 23-fold occurred at 4.76 J/cm^2, while exposures ⩾4.76 J/cm^2 showed decreased *hsp70* expression. This suggested that significant cell damage was induced in the tissue above this threshold. At 6.45 μm, a maximum of 28-fold occurred with the 19.89-J/cm^2 exposure, and with 6.10 μm an 18-fold induction was observed with 17.91 J/cm^2. Of the wavelengths tested, 6.10 μm generated the lowest levels of *hsp70* expression.

3.5 *Correlation Between hsp70 Expression and Collateral Thermal Damage*

In Fig. 6(c), the *hsp70* induction levels are plotted versus the depth of tissue damage. The data showed that 6.10 and 6.45 μm exhibited similar responses (see black lines). The 2.94-μm plot revealed a markedly different trend (see dotted gray line) [Fig. 6(c)]. Compared to the 6-μm wavelengths, the 2.94-μm curve is shifted to the left for lower radiant exposures. Furthermore, at low radiant exposures, the depth of damage increased with increases in *hsp70* expression, but for higher radiant exposures, the depth of damage increased while *hsp70* levels decreased.

3.6 *Epidermal Hyperplasia in Laser-Treated Tissues*

Pronounced thickening of the epidermis, or epidermal hyperplasia, can be used as an indicator of a more intense or persistent repair response, presumably caused by a more damaging insult. At 120-h postsurgery, tissue treated with a wavelength of 6.10 μm showed the least amount of epidermal thickening. For all wavelengths tested, the degree of epidermal hyperplasia was generally dose-dependent. Laser-treated tissues for each treatment wavelength using a radiant exposure of 11.94 J/cm^2 are illustrated [Figs. 7(a)–7(d)]. The tissue treated with 6.10 μm showed minimal epidermal hyperplasia; however, at the same radiant exposure, both 6.45- and 2.94-μm treatments showed 2× more hyperplasia than the 6.10-μm treatment [Figs. 7(b)–7(d)]. In Fig. 7(e), the magnitude of epidermal thickening is plotted versus the laser radiant exposure. At the lowest radiant exposure (7.96 J/cm^2), each treatment wavelength demonstrated similar degrees of epidermal hyperplasia (~4–5× thicker). Maximal epidermal thickening of 10-fold resulted from a wavelength of 2.94 μm and a radiant exposure of 19.89 J/cm^2. The magnitude of hyperplasia at 6.10 μm was statistically lower than the other wavelengths.

4 Discussion

In this study, we sought to determine the superior mid-IR wavelength for the laser ablation of skin. We hypothesized that specific wavelengths of IR light that target both protein and water absorption would achieve less thermal damage than those targeting water absorption alone. To test this hypothesis, we tuned the FEL to water absorbing (2.94 μm) and protein and water absorbing wavelengths (6.10 and 6.45 μm). The ensuing collateral tissue damage was then assessed using optical imaging and traditional histological methods. The magnitude of *hsp70* promoter activity, which was used as a surrogate marker for sublethal cellular damage, was found to be dose- and wavelength-dependent. Compared to other wavelengths, tissues treated with 6.10 μm showed the lowest *hsp70* expression levels, the shallowest depth of damage, and the least amount of epidermal thickening. Therefore, compared to 2.94 and 6.45 μm, the 6.10-μm wavelength proves to be the optimum ablation wavelength in dermal tissue.

4.1 *Laser Surgical Ablation*

Laser sources in the IR (2 to 10 μm) are well suited for ablation procedures, and studies have shown that wavelengths that target protein absorption (6.10 and 6.45 μm) may be

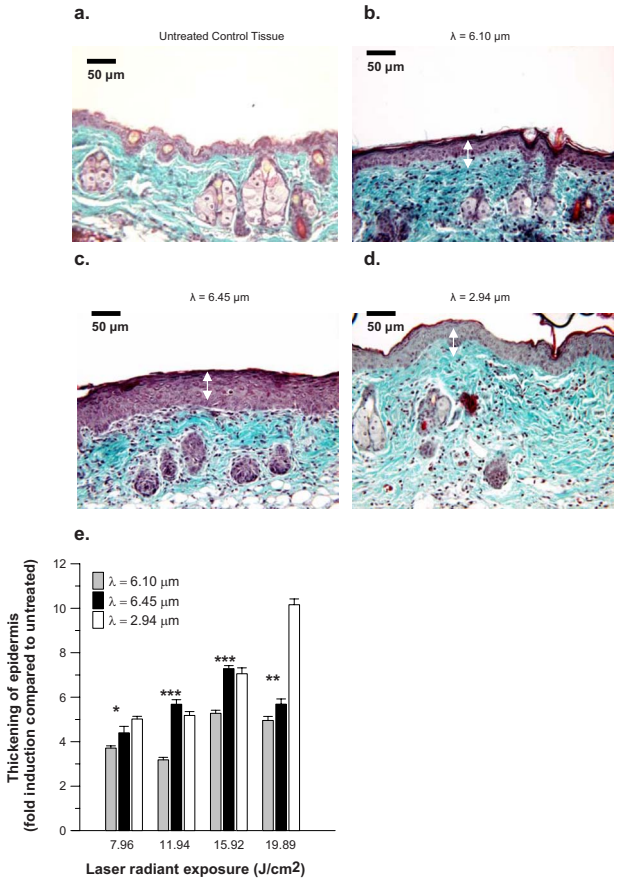

Fig. 7 Epidermal hyperplasia: an early wound repair response in laser-treated tissues. (a–d) Sample representation of Gomori trichrome stains of tissues evaluated 120-h postsurgery (scale bar=50 μm). (a) Untreated tissue, (b) λ=6.10 μm, (c) λ=6.45 μm, and (d) λ=2.94 μm. All tissues were treated with a radiant exposure of 11.94 J/cm^2. The 6.10 μm generated the least amount of epidermal thickening. (Note: arrow demarcates the zone of epidermal hyperplasia.) (e) The magnitude of epidermal thickening 120 h after FEL exposure is plotted versus the radiant exposure for each wavelength. (Note: untreated tissue has an average thickness of 20 μm). The magnitude of epidermal thickening is expressed as the mean±SEM. Samples were compared using a student's t-test (*=P<0.01, **=P<0.005, ***=P<0.001, and n=25).

more effective than wavelengths that target nonspecific water absorption (2.94 μm). However, in most tissues including skin, it is still unclear which IR wavelength is superior. Many biophysical studies have been conducted to elucidate the mechanism governing the removal of tissue in ablation procedures.[9,10,21,34,35] However, few studies have examined the repair response of the tissue that remains after ablation.

In this study, we have used a unique approach to examine the biological effects that are associated with IR laser ablation. In contrast to traditional studies, which typically have used only histological tools to assess collateral damage on excised tissues, we have used optical imaging techniques to quantify damage on the skin of an intact live organism.[8,21]

In addition to providing repair response information, the optical imaging tools used in this study also gave us the ability to quantify the cellular response to thermal stress in a sensitive and noninvasive manner. Traditionally, histological tools are used to examine the severe damage that is generated in the tissue's extracellular matrix (ECM). Bearing in mind that the cell ultimately dictates the fate of the laser-treated tissue, we suggest that it may be more informative to focus on the thermal response of the cell rather than that of the ECM. In addition, intracellular protein damage, which drives the transcriptional activation of heat shock genes, only requires temperature increases of ~5 °C; while peak transition temperatures ≥20 °C are required for ECM proteins to denature.[28,36] In contrast to conventional histology alone, the BLI of the *hsp70-luc-GFP* reporter gene in a transgenic mouse model, in combination with histology, gave us the additional ability to distinguish lethal from sublethal thermal damage.

4.2 *Advantages of Using Multimodal Optical Imaging Techniques*

To ascertain a greater wealth of biological information in this study, we used both bioluminescence imaging (BLI) and fluorescence imaging (FLI) to visualize *hsp70* expression. The primary advantage of BLI is that it can be used to detect and quantify very low levels of light from relatively deep tissue sources. In fact, studies have reported that as few as 200 cells can be detected at a depth of ~2 cm in an *in vivo* mouse model.[37] Mouse dermis is roughly 300 μm thick, so for this study bioluminescence techniques are well suited to measure the emission of light from the entire FEL-treated tissue zone. However, since the BLI images in this study are 2-D and lack depth information, FLI was useful for examining the *hsp70* levels with respect to precise lateral spatial location (x,y) and depth (z). An additional advantage of FLI is unlike BLI, it does not require a live tissue and can be measured postmortem on fixed tissues. Overall, these properties make combined BLI and FLI ideal for visual representation, spatio-temporal characterization, and quantification of *hsp70* driven reporter activity in FEL wounds.

4.3 *Collateral Tissue Damage*

Tissue temperatures are reported to exceed 400 °C during laser ablation procedures.[38] These elevated temperatures cause collagen to denature, water to vaporize, and organic matter to decompose. Collagen denaturation, an irreversible kinetic process, is primarily governed by the temperature-time history and specimen hydration level.[39] Collagen typically denatures at ~60 °C within minutes and at ~68 °C within seconds.[40] Traditionally in ablation studies, the degree of collateral damage is reported using the measured depth of collagen denaturation. In this study, we have shown that for all wavelengths, increases in the radiant exposure caused increases in collateral damage. Of the wavelengths tested, the 6.10-μm wavelength induced the least collateral damage, roughly half that of 6.45 μm and a third that of 2.94 μm. This finding is consistent with that observed by other authors in the cornea.[8,26] The finding that 2.94 μm caused the deepest damage yet has the smallest δ seems counterintuitive, but other studies have also reported similar results.[17,19,20] Spectroscopic investigations have shown that the μ_a of water changes during laser treatment, thus the δ at 2.94 μm may actually be 5 to 10× higher than predicted.[17,19,20] Thus, the dynamic optical properties of tissue may contribute to the deeper damage

induced at 2.94 μm. Also, since 2.94 μm targets the OH-stretch mode (water absorption peak), this wavelength may also cause greater tissue dehydration, increasing the rate of collagen denaturation and the degree of damage.[39] Lastly, given that the pulse duration equals 5 μs, conditions for thermal confinement are not met for the 2.94-μm wavelength ($\tau_{th}=1.67\times10^{-6}$ s), but are met for the 6.10- and 6.45-μm wavelengths (2.67×10^{-5} s and 2.4×10^{-4} s, respectively). Thermal superposition owing to multiple pulses may further complicate the temperature-time history dynamics.

4.4 *Using hsp70 Luciferase Green Fluorescent Protein Systems to Measure Sublethal Thermal Effects*

Since the more subtle effects of cellular thermal damage are not distinguishable with histological methods, the noninvasive readout of *hsp70* levels were used to assess the magnitude of sublethal thermal damage. In a previous study with a skin equivalent model, we showed that the *hsp70* levels rose to a maximum with increasing laser exposures.[30,31,41] Here we also found a similar biphasic behavior. Consistent with the histological data, the BLI data showed that 6.45 μm ($\delta\sim12$ μm) induced $\sim2\times$ higher *hsp70* expression than 6.10 μm ($\delta\sim4$ μm). Besides the δ, the direct targeting of extracellular and/or intracellular proteins could also account for the higher *hsp70* levels. Since 6.45 μm targets the amide-II band of proteins, both intra- and extracellular, this targeting may cause greater protein denaturation than 6.10 μm, which targets the amide-I band. Such targeting may generate more stress to the cells that remain after ablation.

Nevertheless, a Beer's law approximation using the estimated δ in Table 1[42] cannot account for the exceedingly high *hsp70* levels observed at 2.94 μm using $H\leqslant4.76$ J/cm^2. Based on the lower δ, we anticipated that the *hsp70* levels at 2.94 μm would be the lowest of the wavelengths tested. The data suggest that tissue damage and *hsp70* expression are not directly proportional for all wavelengths. Both mid-IR wavelengths (6.45 and 6.10 μm) had similar linear relationships between these two parameters; however, for 2.94 μm, hsp70 expression and depth of damage showed a markedly different relationship. The curve is shifted to the left for low radiant exposures (<4.76 J/cm^2), indicating that greater cellular injury (*hsp70* magnitude) is triggered for a given depth of tissue damage. For instance, to generate 90 μm of tissue damage, 5 J/cm^2 is needed at 2.94 μm, while 8 J/cm^2 is required at 6.45 μm [Fig. 6(a)]. Thus, for the same depth of measured histological damage, 2.94 μm had $\sim2\times$ higher *hsp70* expression than 6.45 μm [Fig. 6(c)]. In addition, at higher radiant exposures, the 2.94-μm curve shows a decline in hsp70 expression, while the depth of damage increases. This change is presumably due to severe thermal effects that impair hsp70 transcription or translation. Taken together, these findings suggest that 2.94 μm causes more severe thermal insult to cells than 6.10 and 6.45 μm. Overall, it appears that *hsp70* expression is influenced by both the δ and the specific constituent (biomolecule) that a laser wavelength targets.

4.5 *Defining Lethal Expression Thresholds with hsp70 Expression*

Due to the more severe and deeper damage, radiant exposures $\geqslant4.76$ J/cm^2 at 2.94 μm resulted in decreases in *hsp70* expression. Unlike the other mid-IR wavelengths, 2.94 μm generated visual damage that included bleeding and coagulation, during and immediately after laser exposure. Therefore, the decreasing hsp70 levels may be due to lethal cell damage or generation of more chromophores (e.g., blood or eschar) that absorb the emitted underlying BLI signal ($\lambda_{emission}=590\pm70$ nm). At a given radiant exposure, the 2.94-μm wavelength is expected to generate higher tissue temperatures than the other wavelengths, owing to the higher μ_a since ΔT is proportional to μ_a.[43] These higher temperatures drive heat conduction and may cause greater photothermal damage. Such damage may impair the cell and perhaps the cellular machinery that makes the bioluminescence reaction possible. Since the bioluminescence reaction requires ATP as a cofactor, damage to the mitochondria (which occurs at $T\geqslant50$ °C) may reduce the efficiency of the reaction and thereby reduce the light emission.[29,44]

To classify these findings, we defined a lethal *hsp70* expression threshold value, hereafter referred to as $hsp70_{L\text{-Th}}$. We define the $hsp70_{L\text{-Th}}$ as the radiant exposure required to cause a decrease in *hsp70* levels. For the radiant exposures listed, the 2.94-μm wavelength had an $hsp70_{L\text{-Th}}$ at ($H\geqslant4.76$ J/cm^2), while the protein targeting wavelengths did not have observable thresholds, at least not for the maximum radiant exposures achievable with the FEL. Overall, the BLI approach is not applicable at extremely destructive laser exposures, and in those cases histology provides a proven method of assessing tissue damage.

4.6 *Wound Repair Response*

The finding that the temporal expression kinetics of *hsp70* are affected by the laser wavelength suggests that the tissue's repair response is wavelength-dependent. Tissues treated with 6.45 μm exhibited bimodal peaks occurring $\sim$9 to 12 and $\sim$24 h after surgery, while the tissues treated with 6.10 and 2.94 μm had only one maximum occurring 9 to 12 h after surgery. This could be due to the greater δ or to the relatively higher absorption by proteins at 6.45 μm. Later wound repair also appears to be wavelength-dependent. Five days after laser surgery, we evaluated the magnitude of epidermal hyperplasia, which is a transient characteristic of the resurfacing phase of skin repair. In the context of the present study, reduced hyperplasia was indicative of a less severe wound, and the 6.10-μm wavelength was superior in this aspect.

4.7 *Broader Implications of Findings*

Nearly 15 years ago, the 6.45-μm wavelength was shown to cause minimal collateral damage in excised tissue.[21] More recent evidence has suggested that 6.1 μm is superior to 6.45 μm.[8,9,26] In this study, we have also found that 6.10 μm was superior to 6.45 and 2.94 μm. Previous studies have reported that the difference between 6.45 and 6.10 μm was not clinically significant (7 versus 5 μm, respectively).[26] In contrast, in this work, where we conduct ablation on intact live animals, we have shown that the differences in tissue damage between 6.45 and 6.10 μm are of practical importance (90 versus 50 μm, respectively). Since dermal stratum are roughly 20 μm thick, using 6.10 μm may allow for more controlled ablation. In addition, this work has also shown that 2.94 μm was markedly inferior to both 6-μm wavelengths.

Considering the limited clinical utility of the FEL, the implications of these findings are significant. The FEL requires high costs to operate and has practical limitations in terms of beam delivery. The development of low-cost benchtop laser sources, based on a variety of solid-state platforms, may increase the clinical use of lasers for surgical ablation. Since surgical performance is primarily governed by the selection of the laser's pulse structure, wavelength, and radiant exposure,[8–10] studies like the work presented here help assist in the development of these alternative sources. Recent reports have shown that the micropulse structure is not a critical parameter that needs to be duplicated in benchtop laser sources.[9] The data in this report suggest that efforts in developing laser sources using 6-μm radiation, such as using the zinc germanium phosphide optical parametric oscillator or systems based on stimulated Raman scattering, are useful cost-effective alternatives to the FEL, and should be further pursued.[26,45]

In a broader sense, this study also demonstrates that using multimodal optical imaging techniques in a transgenic mouse model (*hsp70*-L2G) can aid in the assessment of the biological response in surgical ablation procedures. The bioluminescence data demonstrates that the magnitude of *hsp70* expression was both dose and wavelength-dependent. While many previous studies have used optical imaging techniques to visualize the promoter activity of genes involved in cutaneous wound repair, this study reveals that the *hsp70* mouse is a particularly useful tool for investigating laser-tissue interactions.[46–48] This type of model may be effective in connecting our knowledge of the biophysics of the ablation process to the histological assessments of laser-treated tissues. Ultimately, this model can be used to improve laser surgical procedures, including a variety of dermatological aesthetic laser procedures, such as skin resurfacing.

Acknowledgments

We wish to thank John Kozub and the FEL staff for their assistance. We also wish to thank Evelyn Okediji for her histology expertise. We also wish to thank the personnel of the Skin Disease and Research Center and specifically the Immunohistochemistry Core. These studies were supported by the DOD MFEL program (F49620-01-1-0429 and FA9550-04-1-0045) and the NIH Skin Disease Research Core Centers (SDRCC) (5P30 AR041043), Department of Veteran Affairs (JMD).

References

1. L. Goldman, *Biomedical Aspects of the Laser. The Introduction of Laser Applications into Biology and Medicine*, Berlin (1967).
2. L. Goldman, *Applications of the Laser*, CRC Press, Boca Raton, FL (1973).
3. R. R. Anderson and J. A. Parrish, "Selective photothermolysis: precise microsurgery by selective absorption of pulsed radiation," *Science* **220**(4596), 524–527 (1983).
4. M. Wolbarsht, *Laser Applications in Medicine and Biology*, p. 255–274, Plenum, New York (1971).
5. M. Wolbarsht, "Laser surgery: CO_2 or HF," *IEEE J. Quantum Electron.* **20**(12), 1427–1432 (1984).
6. R. Srinivasan, "Ablation of polymers and biological tissue by ultraviolet lasers," *Science*, **234**(4776), 559–565 (1986).
7. R. J. Lane et al., "Ultraviolet-laser ablation of skin," *Arch. Dermatol.* **121**(5), 609–617 (1985).
8. M. A. Mackanos et al., "The effect of free-electron laser pulse structure on mid-infrared soft-tissue ablation: biological effects," *Phys. Med. Biol.* **50**(8), 1885–1899 (2005).
9. M. A. Mackanos, J. A. Kozub, and E. D. Jansen, "The effect of free-electron laser pulse structure on mid-infrared soft-tissue ablation: ablation metrics," *Phys. Med. Biol.* **50**(8), 1871–1883 (2005).
10. M. S. Hutson et al., "Advances in the physical understanding of laser surgery at 6.45 microns," *Intl. Free Electron Laser Conf.* 648–653 (2004).
11. G. Q. Hale, "MR, Optical constants of water in 200 nm to 200 μm wavelength region," *Appl. Opt.* **12**(3), 555–563 (1973).
12. J. T. Walsh, Jr. and T. F. Deutsch, "Pulsed CO2 laser tissue ablation: measurement of the ablation rate," *Lasers Surg. Med.* **8**(3), 264–275 (1988).
13. M. Speyer et al., "Thermal injury patterns and tensile strength of canine oral mucosa after carbon dioxide laser incisions," *Laryngoscope* **106**(7), 845–850 (1996).
14. D. L. Sanders and L. Reinisch, "Wound healing and collagen thermal damage in 7.5-microsec pulsed CO(2) laser skin incisions," *Lasers Surg. Med.* **26**(1), 22–32 (2000).
15. J. P. Cochrane et al., "Wound healing after laser surgery: an experimental study," *Br. J. Surg.* **67**(10), 740–743 (1980).
16. Y. M. Molgat et al., "Comparative study of wound healing in porcine skin with CO2 laser and other surgical modalities: preliminary findings," *Int. J. Dermatol.* **34**(1), 42–47 (1995).
17. J. T. Walsh, Jr., T. J. Flotte, and T. F. Deutsch, "Er:YAG laser ablation of tissue: effect of pulse duration and tissue type on thermal damage," *Lasers Surg. Med.* **9**(4), 314–326 (1989).
18. J. T. Walsh, Jr. and T. F. Deutsch, "Er:YAG laser ablation of tissue: measurement of ablation rates," *Lasers Surg. Med.* **9**(4), 327–337 (1989).
19. Vodop'yanov et al., "A change in the refractive properties of water irradiated by a 2.94-?m erbium laser," *Quantum Electron.* **30**(11), 975–978 (2000).
20. J. T. Walsh, Jr. and J. P. Cummings, "Effect of the dynamic optical properties of water on midinfrared laser ablation," *Lasers Surg. Med.* **15**(3), 295–305 (1994).
21. G. Edwards et al., "Tissue ablation by a free-electron laser tuned to the amide II band," *Nature (London)* **371**(6496), 416–419 (1994).
22. K. M. Joos et al., "Optic nerve sheath fenestration with endoscopic accessory instruments versus the free electron laser (FEL)," *Lasers Surg. Med.* **38**(9), 846–851 (2006).
23. L. A. Mawn et al., "Development of an orbital endoscope for use with the free electron laser," *Ophthal Plast. Reconstr Surg.* **20**(2), 150–157 (2004).
24. K. M. Joos et al., "Chronic and acute analysis of optic nerve sheath fenestration with the free electron laser in monkeys," *Lasers Surg. Med.* **32**(1), 32–41 (2003).
25. K. M. Joos et al., "Optic nerve sheath fenestration with a novel wavelength produced by the free electron laser (FEL)," *Lasers Surg. Med.* **27**(3), 191–205 (2000).
26. M. A. Mackanos et al., "Mid infrared optical parametric oscillator (OPO) as a viable alternative to tissue ablation with the free electron laser (FEL)," *Lasers Surg. Med.* **39**(3), 230–236 (2007).
27. D. L. Ellis et al., "Free electron laser infrared wavelength specificity for cutaneous contraction," *Lasers Surg. Med.* **25**(1), 1–7 (1999).
28. R. I. Morimoto, P. E. Kroeger, and J. J. Cotto, "The transcriptional regulation of heat shock genes: a plethora of heat shock factors and regulatory conditions," *EXS* **77**, 139–163 (1996).
29. C. E. O'Connell-Rodwell et al., "A genetic reporter of thermal stress defines physiologic zones over a defined temperature range," *FASEB J.* **18**(2), 264–271 (2004).
30. J. T. Beckham et al., "Assessment of cellular response to thermal laser injury through bioluminescence imaging of heat shock protein 70," *Photochem. Photobiol.* **79**(1), 76–85 (2004).
31. G. J. Wilmink et al., "Assessing laser-tissue damage with bioluminescent imaging," *J. Biomed. Opt.* **11**(4), 041114 (2006).
32. M. M. O'Connell-Rodwell, D. M. Simanovskii, Y. A. Cao, M. E. Bachmann, H. A. Schwettman, and C. H. Contag, "In vivo analysis of Hsp70 induction following pulsed laser irradiation in a transgenic reporter mouse," *J. Biomed. Opt.* **13**(3), 030501 (2008).
33. L. Reinisch et al., "Computer-assisted surgical techniques using the Vanderbilt free electron laser," *Laryngoscope* **104**(11 Pt 1), 1323–1329 (1994).
34. G. S. Edwards and M. S. Hutson, "Advantage of the Mark-III FEL

for biophysical research and biomedical applications," *J. Synchrotron Radiat.* **10**(5), 354–357 (2003).
35. G. L. Bryant et al., "Histologic study of oral mucosa wound healing: a comparison of a 6.0- to 6.8-micrometer pulsed laser and a carbon dioxide laser," *Laryngoscope* **108**(1 Pt 1), 13–17 (1998).
36. P. E. McClain and E. R. Wiley, "Differential scanning calorimeter studies of the thermal transitions of collagen. Implications on structure and stability," *J. Biol. Chem.* **247**(3), 692–697 (1972).
37. T. Troy et al., "Quantitative comparison of the sensitivity of detection of fluorescent and bioluminescent reporters in animal models," *Mol. Imaging* **3**(1), 9–23 (2004).
38. D. M. Harris et al., "Eyelid resurfacing," *Lasers Surg. Med.* **25**(2), 107–122 (1999).
39. N. T. Wright and J. D. Humphrey, "Denaturation of collagen via heating: an irreversible rate process," *Annu. Rev. Biomed. Eng.* **4**, 109–128 (2002).
40. J. C. Allain et al., "Isometric tensions developed during the hydrothermal swelling of rat skin," *Connect. Tissue Res.* **7**(3), 127–133 (1980).
41. G. J. Wilmink, S. R. Opalenik, J. T. Beckham, A. A. Abraham, L. B. Nanney, A. Mahadevan-Jansen, J. M. Davidson, and E. D. Jansen, "Molecular imaging-assisted optimization of Hsp70 expression during laser-induced thermal preconditioning for wound repair enhancement," (Nature Publishing Group, 2008).
42. W. S. Wieliczka and M. R. Querry, "Wedge shaped cell for highly absorbent liquids: infrared optical constants of water," *Appl. Opt.* **28**, 1714 (1989).
43. A. J. Welch and M. J. C. v. Gemert, "Optical-thermal response of laser-irradiated tissue," in *Lasers, Photonics, and Electro-Optics*, Plenum Press, New York (1995).
44. T. Y. Tsong and Z. D. Su, "Biological effects of electric shock and heat denaturation and oxidation of molecules, membranes, and cellular functions," *Ann. N.Y. Acad. Sci.* **888**, 211–232 (1999).
45. G. S. Edwards et al., "6450 nm wavelength tissue ablation using a nanosecond laser based on difference frequency mixing and stimulated Raman scattering," *Opt. Lett.* **32**(11), 1426–1428 (2007).
46. N. Wu et al., "Real-time visualization of MMP-13 promoter activity in transgenic mice," *Matrix Biol.* **21**(2), 149–161 (2002).
47. N. Wu, E. D. Jansen, and J. M. Davidson, "Comparison of mouse matrix metalloproteinase 13 expression in free-electron laser and scalpel incisions during wound healing," *J. Invest. Dermatol.* **121**(4), 926–932 (2003).
48. A. D. Izzo et al., "In vivo optical imaging of expression of vascular endothelial growth factor following laser incision in skin," *Lasers Surg. Med.* **29**(4), 343–350 (2001).